Published in final edited form as:
Dev Cell. 2008 October ; 15(4): 509–520. doi:10.1016/j.devcel.2008.07.017.

The endoderm of the mouse embryo arises by dynamic widespread intercalation of embryonic and extraembryonic lineages

Gloria S. Kwon[1,2], **Manuel Viotti**[1,3], and **Anna-Katerina Hadjantonakis**[1,4]

1*Developmental Biology Program, Sloan-Kettering Institute, 1275 York Avenue, New York, New York 10021, USA.*

2*Neuroscience Program, Weill Graduate School of Medical Sciences of Cornell University, New York, NY 10021, USA.*

3*Biochemistry, Cell and Molecular Biology Program, Weill Graduate School of Medical Sciences of Cornell University, New York, NY 10021, USA.*

SUMMARY

The cell movements underlying the morphogenesis of the embryonic endoderm, the tissue that will give rise to the respiratory and digestive tracts, are complex and not well understood. Using live imaging combined with genetic labeling, we investigated the cell behaviors and fate of the visceral endoderm during endoderm formation in the mouse gastrula. Contrary to the prevailing view, our data reveal no mass displacement of visceral endoderm to extraembryonic regions concomitant with the emergence of epiblast-derived definitive endoderm. Instead, we observed dispersal of the visceral endoderm epithelium and extensive mixing between cells of visceral endoderm and epiblast origin. Visceral endoderm cells remained associated with the epiblast and were incorporated into the early gut tube. Our findings suggest that the segregation of extraembryonic and embryonic tissues within the mammalian embryo are not as strict as believed, and that a lineage previously defined as exclusively extraembryonic contributes cells to the embryo.

Keywords

mouse embryo; visceral endoderm; epiblast; definitive endoderm; gastrulation; primitive streak; live imaging; fluorescent protein; alpha-fetoprotein; transthyretin; transgenic; chimera

INTRODUCTION

In the mouse, gastrulation is the event that results in the formation of the three germ layers from the pluripotent epiblast and leads to the elaboration of the embryonic axes. Prior to the initiation of gastrulation, the mouse embryo comprises a bilaminar cup-shaped structure consisting of visceral endoderm and the epiblast, which will give rise to the fetus and extraembryonic mesoderm. The visceral endoderm is involved in nutrient uptake and transport

4Author for correspondence., E-mail: hadj@mskcc.org (Email), 1-212-639-3159 (Phone), 1-646-422-2355 (FAX).

and also plays a critical role in the morphogenesis and patterning of the epiblast (Hogan and Zaret, 2002; Srinivas, 2006). There is increasing evidence for extensive cellular heterogeneity, dynamic cell behaviors and intrinsic cell polarity within the visceral endoderm (Mesnard et al., 2006; Rivera-Perez et al., 2003; Rivera-Perez and Magnuson, 2005; Rodriguez et al., 2005; Thomas and Beddington, 1996).

The visceral endoderm set aside as a lineage in the late blastocyst, in contrast to the definitive endoderm which arises from the epiblast at gastrulation. It is thought that the visceral endoderm is fated to form the endoderm of the extraembryonic visceral yolk sac, whereas the definitive endoderm exclusively represents the embryonic endoderm, giving rise to the epithelial lining of the respiratory and digestive tracts and their associated organs including the lungs, liver and pancreas (Hogan and Zaret, 2002).

At gastrulation, cells that will form the mesoderm and definitive endoderm are recruited from the epiblast and ingress through the primitive streak, a morphologically distinct structure which marks the posterior end of the embryo. Mesoderm emanates from the primitive streak as two bilateral wings of cells that spread anteriorly as they circumnavigate the space between two epithelia: the visceral endoderm on the outer surface of the embryo and the inner epiblast (Kinder et al., 1999; Lawson et al., 1991; Parameswaran and Tam, 1995; Tam and Beddington, 1987). In contrast to mesoderm, the cell movements underlying the morphogenesis of the definitive endoderm are not well understood (Lewis and Tam, 2006).

Fate-mapping experiments performed by single-cell labeling, embryo painting and cell transplantation have revealed that the definitive endoderm is derived from cells that occupy a distal position within the pre-streak (PS) to mid-streak (MS) epiblast (Lawson et al., 1986; Lawson and Pedersen, 1987; Tam and Beddington, 1987; Tam and Beddington, 1992). Studies on pre-streak to early streak (PS-ES) stage embryos suggested the visceral endoderm is displaced proximally by cells that derive from the anterior primitive streak (Lawson et al., 1986). By the early to late bud (EB-LB) stage, visceral endoderm cells in proximal regions contributed to the yolk sac and yolk sac-embryo junction (Lawson et al., 1986; Tam et al., 2004). Further support for the proximal-ward movement of the visceral endoderm comes from the analysis of pan-visceral endoderm markers, which initially mark the cells overlying both embryonic and extraembryonic regions at PS-ES stages, and are subsequently restricted to the visceral layer of the yolk sac at the no bud to early headfold (OB-EHF) stages (Downs and Davies, 1993; Duncan et al., 1994; Tam et al., 2004).

The prevailing model suggests that definitive endoderm cells reach the outer surface of the embryo by inserting into and establishing a congruent epithelium with the pre-existing visceral endoderm cell layer at the distal tip of the embryo. The proposed unidirectional (distal to proximal) displacement of the layer of cells at the surface of the embryo involves the active expansion of the definitive endoderm that pushes the adjacent epithelium of the visceral endoderm proximally towards extraembryonic regions (Hogan and Zaret, 2002). By the late-streak (LS) stage, the endodermal layer overlying the epiblast is believed to be exclusively populated by the definitive endoderm, except for a region overlying the posterior primitive streak (Lawson et al., 1986; Lawson and Pedersen, 1987; Tam and Beddington, 1992). Soon after its formation, the definitive endoderm folds and is internalized to form the gut tube (Hogan and Zaret, 2002; Tremblay and Zaret, 2005) from which the respiratory and digestive tracts, and associated visceral organs will develop (Wells and Melton, 1999).

Because no previous studies have examined the morphogenetic events underlying this process with a high degree of spatial or temporal resolution, little is known of the precise sequence of events and the cell behaviors involved. Anticipating that the events surrounding endoderm formation would be rapid and dynamic, we adopted a live imaging approach to investigate

endoderm morphogenesis (Hadjantonakis et al., 2003). Our strategy involved genetic labeling of the entire visceral endoderm lineage for visualization of cells at high-resolution in individual embryos and at multiple time-points. To label the entire visceral endoderm we used the *Afp::GFP* strain of mice (Kwon et al., 2006), in which the enhanced fluorescent protein variant, *EGFP,* was placed downstream of cis-regulatory elements from the mouse *Alpha-fetoprotein* (*Afp*) locus (Andrews et al., 1982; Krumlauf et al., 1985; Kwon et al., 2006; Tilghman and Belayew, 1982).

Our results reveal a complex series of events that results in extensive mixing between the visceral endoderm and epiblast lineages during the morphogenesis of endoderm. At MS-LS stages, the visceral endoderm epithelium overlying the epiblast is dispersed concomitant with the intercalation of cells originating in the epiblast. Visceral endoderm cells are not displaced to extraembryonic regions. Instead, they remain in association with the epiblast and constitute a subpopulation of cells contributing to the gut tube. These dispersed visceral endoderm derived-cells are organized around distinct morphological signaling centers of the embryo, including the primitive streak, node and midline. Taken together, our experiments provide the first glimpse of the live cell behaviors during endoderm morphogenesis in the mouse. Furthermore they uncover a lineage relationship between the visceral endoderm of the early postimplantation mouse embryo and the endoderm-derived tissues of the fetus and adult.

RESULTS

The uniform epithelium of visceral endoderm overlying the epiblast becomes dispersed by the late streak stage

To visualize visceral endoderm cell dynamics and cell fate during endoderm morphogenesis, we used the *Afp::GFP* strain of mice (Kwon et al., 2006). Live imaging of PS through MS stage *Afp::GFP* embryos confirmed continuous GFP expression exclusively in the surface cell layer, the location of the visceral endoderm (Movie S1). Three-dimensional (3D) rendering of *xyz* data confirmed Afp-GFP$^+$ localization correlated with *Afp* mRNA localization in stage-matched embryos (Figures 1A and 1B, Figure S1A and Movie S2).

Live imaging of embryos from LS through EHF stages (E7.0–E7.5), the time when definitive endoderm emerges (Lin et al., 1994; Tam and Beddington, 1992), revealed a region of continuous Afp-GFP$^+$ cells positioned proximally overlying the extraembryonic ectoderm and proximal epiblast (yellow arrowheads, Figure 1C and 1D), and a distinct distally positioned, dispersed population of Afp-GFP$^+$ cells overlying the distal two thirds of the epiblast (blue arrowheads, Figures 1C and 1D, and Movie S3). The dispersed Afp-GFP$^+$ population represented scattered single cells with irregular morphology (Figure 1E). Posterior views, however, showed a coherent sheet of Afp-GFP$^+$ cells overlying the primitive streak (Figure 1F), likely corresponding to the posterior visceral endoderm (PVE) or its descendents (Rivera-Perez and Magnuson, 2005). These observations contrasted with the prevailing model in which the visceral endoderm is sustained as a contiguous epithelium that is displaced to extraembryonic regions by emergent definitive endoderm.

3D reconstructions of LS-EHF imaging data confirmed that scattered Afp-GFP$^+$ cells persisted on the surface layer of the embryo. By the late headfold (LHF) to early somite (ESom) stages (E7.75–8.25) GFP-negative cells predominated in the surface layer of the embryo. However, individual Afp-GFP$^+$ cells were still present scattered over the distal region of the embryo as visualized in lateral views (Figure 1G and Movie S4), and were more abundant in posterior and distal locations. Posteriorly, Afp-GFP$^+$ cells formed a contiguous sheet of cells overlying the primitive streak (Movie S5), and distally they were organized around the node and anterior midline (Figure 1H and Movie S6).

Labeling the scattered population of cells with independent transgenes supports visceral endoderm origin

To validate that the scattered population of cells overlying the epiblast were of visceral endoderm origin, we generated additional transgenic strains using cis-regulatory elements from another endoderm specific gene, *Transthyretin* (*Ttr*). Cis-regulatory elements from the *Ttr* locus had previously been shown to drive transgene expression within the yolk sac endoderm and fetal liver (Costa et al., 1990). *Ttr* mRNA expression assayed by *in situ* hybridization had also been shown to localize to the entire visceral endoderm at pre-streak stages (Mesnard et al., 2006). Sequence comparisons of the *Afp* and *Ttr* cis-regulatory elements failed to reveal any large regions of homology, so these represented independent reporters of the visceral endoderm lineage.

We generated *Ttr::RFP* strains in which the 3kb upstream region and first exon of *Ttr* was used to drive expression of a monomeric red fluorescent protein (RFP) transgene (Campbell et al., 2002). High-resolution imaging of *Ttr::RFP* embryos demonstrated a correlation of fluorescence with endogenous *Ttr* expression and revealed a scattered population of Ttr-RFP$^+$ cells overlying the epiblast in LS-EB stage embryos (Figure 2A). This cell population resembled the population of Afp-GFP$^+$ cells observed in *Afp::GFP* embryos. To determine whether the same cell population was labeled in the two transgenic strains, we generated double transgenic *Afp::GFP ; Ttr::RFP* embryos. Dispersed double fluorescent (Afp-GFP$^+$; Ttr-RFP$^+$) cells (yellow) predominated over the distal two thirds of the epiblast, confirming that the same cell population is labeled in both transgenic strains (Figure 2B).

Fluorescent protein reporter perdures in cells overlying the epiblast

Our findings suggested that either visceral endoderm cells became dispersed but remained overlying the epiblast, or that the *Afp::GFP* transgene was activated within a sub-population of epiblast-derived cells that occupied the outermost layer of the embryo overlying the epiblast. Support for the prevailing model of endoderm formation comes from the analysis of molecular markers (such as *Afp* and *Ttr* mRNAs), which are documented as either encompassing the entire epiblast (PS-MS stages) or being fully displaced (LS-EB stages). Our live imaging observations were in disagreement with these data. We therefore compared the localization of Afp-GFP$^+$ cells to *GFP* mRNA in *Afp::GFP* embryos. We live imaged consecutively staged PS-EHF embryos (~E5.75–E7.5), then processed them for wholemount *GFP* mRNA *in situ* hybridization (Figures 2C–2F). This allowed us to determine whether GFP fluorescence was due to perdurance of the fluorescent protein in cells that were derived from the visceral endoderm. It would also reveal whether the *Afp cis*-regulatory elements active within visceral endoderm cells were not responsive to downregulation or if the *Afp::GFP* transgene was being activated in epiblast-derived cells in the outermost layer of the embryo.

At PS-ES stages (E5.75–6.25), GFP protein localization tightly correlated with *GFP* mRNA in *Afp::GFP* embryos, being widespread throughout the visceral endoderm (Figures 2C and 2D). However by the LS-EB stages, when Afp-GFP$^+$ cells changed to a contiguous sheet overlying the extraembryonic ectoderm and proximal epiblast, and a scattered population of cells overlying the distal two thirds of the epiblast, *GFP* mRNA was detected only in the visceral endoderm overlying extraembryonic regions and proximal epiblast (Figures 2E and 2F). This indicates that GFP protein perdures and functions as a short-term lineage tracer in *Afp::GFP* embryos, and that scattered Afp-GFP$^+$ cells overlying the epiblast originate within the visceral endoderm.

To confirm that the scattered population of cells on the embryo surface was not due to heterogeneity in transgene expression, whereby neighboring visceral endoderm-derived cells exhibit concerted downregulation of cis-regulatory elements, we generated an additional

transgenic strain where Cre recombinase was placed downstream of the *Ttr* regulatory elements. Identical results were obtained when the *Ttr::Cre* strain was crossed to either GFP-based or LacZ-based Cre reporter strains. At PS stages, the entire visceral endoderm was labeled with the Cre reporter in agreement with observations made with the *Afp::GFP* and *Ttr::RFP* transgenes (Figure 2G). By the EB stage, a dispersed population of Cre reporter expressing cells remained overlying the epiblast in *Ttr::Cre* embryos (Figure 2H). These data confirm that concerted downregulation of the *Afp::GFP* and *Ttr::RFP* transgenes did not occur, that the scattered population of cells overlying the epiblast are visceral endoderm-derived, and that neighboring cells are of a different origin.

Absence of visceral endoderm markers is due to downregulation of gene expression and not mass cell movements

When investigating *Afp* and *Ttr* mRNA expression (Law and Dugaiczyk, 1981; Yamamura et al., 1985) in whole mount *in situ* preparations of LS-EB stage embryos, the time during which the visceral endoderm became dispersed, a small percentage of embryos exhibited speckled staining overlying the epiblast (black arrowheads, Figure S1A) in all batches of embryos examined. Although this type of coloration might commonly be overlooked and attributed to non-specific background staining, it may instead reveal a rapid downregulation of marker expression.

To determine whether scattered Afp-GFP$^+$ cells overlying the epiblast expressed markers of the visceral endoderm, we analyzed the mRNA expression and protein distribution of *Hnf4α*, a visceral endoderm marker in PS-EB stage (E5.75–E7.5) embryos (Chen et al., 1994; Duncan et al., 1994; Taraviras et al., 1994). Low magnification wholemount imaging revealed that both *Hnf4α* mRNA and protein, which were localized throughout the visceral endoderm overlying both the epiblast and extraembryonic ectoderm at PS-ES stages (E5.75–E6.0), were downregulated in regions overlying the epiblast by the MS-LS stage (E6.5–7.0), and were localized proximally by the EB stage (E7.25–7.5) (Figures 2I, 2M, 2Q and Figure S1).

We confirmed that Hnf4α protein co-localized with GFP, and was restricted to the surface layer of the embryo (Figure S1). High-magnification co-visualization and quantification of Hnf4α protein and GFP in *Afp::GFP* embryos revealed that at the PS stage, all Afp-GFP$^+$ cells exhibited nuclear-localized Hnf4α staining at equal levels (Figures 2J–2L). By the MS stage, even though Hnf4α protein was detected in all cells, those more distally positioned, overlying the epiblast, exhibited reduced levels of protein (white arrowheads, Figures 2N–2P). By the EB stage, Hnf4α protein was predominantly localized proximally overlying the extraembryonic ectoderm (Figures 2R–2T). Close inspection, however, revealed that some scattered Afp-GFP$^+$ cells overlying the proximal epiblast expressed Hnf4α (white arrowheads, Figures 2R–T), but that more distally located Afp-GFP$^+$ cells lacked detectable Hnf4α expression (orange arrowheads, Figures 2S–2T). These data indicate that distally positioned visceral endoderm-derived cells overlying the epiblast downregulate visceral endoderm markers.

Scattered Afp-GFP$^+$ cells overlying the epiblast are not of epiblast origin

To confirm the visceral endoderm origin of cells observed overlying the epiblast in the *Afp* and *Ttr* transgenic strains, we needed to exclude the possibility that cells derived from the epiblast had activated transgene expression. To do this we used three different approaches.

X-inactivation in X^m/X^{pGFP} embryos—First we used an epigenetic approach to label cells of the epiblast by analyzing X^m/X^{pGFP} female embryos carrying a paternally inherited copy of a widely expressed X-linked GFP transgene (Hadjantonakis et al., 1998b). In such embryos, the X^{pGFP} transgene is imprinted, and thus silenced, in cells of the visceral endoderm and

extraembryonic ectoderm, while cells of the epiblast are subject to random X-inactivation resulting in mosaic GFP expression (Hadjantonakis et al., 2001). Imaging of double transgenic X^m/X^{pGFP} ; *Ttr::RFP* OB-EHF stage embryos revealed individual GFP^+ or RFP^+ cells. However no double fluorescent cells were observed in over 200 cells counted (Figures 3A–3H). This indicates that X-GFP^+ and Ttr-RFP^+ cells in the outer layer of the embryo overlying the epiblast have distinct origins.

Cre recombinase-mediated fate mapping—Next we employed a Cre recombinase-mediated genetic fate mapping approach (Lewandoski, 2001). We used two epiblast-specific Cre strains: the *Sox2::Cre* strain, which catalyzes excision in all cells of the epiblast (Hayashi et al., 2002), and the *MORE::Cre* strain, which also catalyzes excision throughout the epiblast, but in a mosaic fashion (Tallquist and Soriano, 2000). These Cre strains were crossed onto the *Z/EG* strain, a *CAG* promoter GFP-based Cre reporter (Novak et al., 2000) and the *Ttr::RFP* strain. We imaged embryos and scored for single GFP^+ or RFP^+ cells along with double GFP^+ ; RFP^+ cells in triple transgenic embryos of the following two genotypes: *Sox2::Cre* ; *Z/EG* ; *Ttr::RFP* (data not shown) and *MORE::Cre* ; *Z/EG* ; *Ttr::RFP* (Figure S2A–F). Although single fluorescent protein expressing cells were detected in all embryos, we were unable to identify any double fluorescent protein cells in over 200 cells counted. These data indicate that GFP^+ and RFP^+ cells represent distinct lineages and are either of epiblast or visceral endoderm origin respectively. These data supported our conclusions from X^m/X^{pGFP} embryos.

Tetraploid chimeras—Previous experiments with tetraploid (4n) chimeras, in which the visceral endoderm and extraembryonic ectoderm lineages are tetraploid and segregated from those of the diploid epiblast (Tam and Rossant, 2003), have suggested that a sub-population of 4n cells may remain associated with the embryonic gut (Dufort et al., 1998; Hadjantonakis et al., 2002). To determine whether 4n endoderm cells represent the same population observed in *Afp::GFP* and *Ttr::RFP* embryos, we generated a series of 4n <-> 2n embryo chimeras (Eakin and Hadjantonakis, 2006; Nagy et al., 1993). The 4n compartment was derived from a *CAG::RFP* strain of mice that exhibits widespread RFP expression (Long et al., 2005). 3D rendering of confocal *z*-stacks acquired from these LB-EHF (E7.5), LHF (E7.75) and ESom (E8.25) chimeras confirmed the presence of a scattered population of 4n cells overlying the epiblast (Figures 3J–L and Figure S2G–L). The morphology and distribution of RFP^+ 4n cells resembled visceral endoderm-derived Afp-GFP^+ and Ttr-RFP^+ cells overlying the epiblast.

Our observations from these three independent approaches lead us to conclude that the scattered population of cells overlying the epiblast are not of epiblast origin, and therefore are derivatives of the visceral endoderm.

Live imaging reveals the progression of visceral endoderm dispersal

To visualize the dynamic sequence of events that culminate in the dispersal of visceral endoderm cells, we generated 3D time-lapse (i.e. 4D) data recordings of *ex utero* cultured embryos (Figure 4A, and Movie S7–Movie S9). Live imaging of LS stage embryos revealed that the initially uniform distribution of GFP (Movie S7), which corresponded to the visceral endoderm overlying both extraembryonic ectoderm and epiblast, was rapidly (<2 hours) transformed by the appearance of small GFP-negative regions. These regions were approximately the size of single cells. We therefore reasoned that the gaps might represent GFP-negative cells that were intercalating with the Afp-GFP^+ cells of the visceral endoderm. GFP-negative regions appeared distally at lateral positions just anterior to the primitive streak. The number and size of these GFP-negative regions increased over the next 6 hours (Figure 4A and Movie S8). Concomitantly, dispersed Afp-GFP^+ cells exhibited an irregular

morphology and not the orthogonal shape that is characteristic of epithelial cells (Figure 1E and 4A, right panel).

We therefore conclude that the visceral endoderm is not displaced by the definitive endoderm as a contiguous epithelial sheet towards extraembryonic regions. Instead, the visceral endoderm epithelium overlying the epiblast undergoes a rapid transformation, and remains overlying the epiblast to become dispersed. Visceral endoderm cell dispersal could be achieved either by growth of the epiblast and its derivatives and/or intercalation by epiblast-derived cells.

Time-lapse imaging of slightly later (EB) stage embryos, in which the scattered population of visceral endoderm-derived cells was already evident, revealed that Afp-GFP$^+$ cells overlying the epiblast exhibited dynamic cell morphologies as they extended and retracted protrusions. However cells did not change position, other than through division or overall embryo growth, and we noted no trend such as a nonorientated/noncoordinated random walk (Pezeron et al., 2008) or directional movement of scattered Afp-GFP$^+$ cells (Movie S9). These live imaging data also confirmed that cell dispersal occurred in the distal two thirds of the visceral endoderm overlying the epiblast, and that the boundary between dispersed and non-dispersed visceral endoderm cells was distal to the position of the embryonic-extraembryonic boundary, as defined by the position of the amnion and the furrow at the cranial half of the embryo (Movie S8). As development proceeded, the position of this morphological boundary between embryonic-extraembryonic regions shifted distally to coincide with the boundary defined by the contiguous versus dispersed population of visceral endoderm-derived cells (Movie S9).

We quantified both the percentage of the surface area of the embryo that was GFP$^+$ and the total number of GFP$^+$ cells overlying the epiblast (including the proximal non-dispersed population), from the ES stage (E6.0) to the LHF stage (E8.0). During this interval, the percent GFP$^+$ area overlying the epiblast decreased over time, from uniform coverage to comprising approximately 25% of the distal surface of the embryo (Figure 4B). During the same time, we noted division of Afp-GFP$^+$ cells within the plane of the epithelium, leading to an increase in the total number of Afp-GFP$^+$ cells (Figure 4C). This indicated that Afp-GFP$^+$ cells were maintained and revealed that, as the embryo grew, the distance between Afp-GFP$^+$ cells increased. It was therefore likely that the dispersal of visceral endoderm-derived cells is due to the rapid increase in the GFP-negative area over that particular developmental window of time.

The dispersed population of Afp-GFP$^+$ cells continues to proliferate

One question that arises from our data is whether the visceral endoderm-derived scattered population of cells overlying the epiblast are maintained or eliminated from the embryo. Live imaging of visceral endoderm-derived cells overlying the epiblast in EHF stage embryos showed cells undergoing division in the plane of the epithelium (Figure S4 and Movie S10). These data indicate that this population expands within the developing embryo and is therefore likely to be maintained. Our time-lapse imaging demonstrated that Afp-GFP$^+$ cell death was negligible (in Movie S10 only 1 cell is seen to die). Absence of Caspase 3 staining at LS-EHF stages (data not shown), supported the maintenance of the Afp-GFP$^+$ cell population. Quantitation of the number of dividing cells revealed that even though visceral endoderm-derived cells overlying the epiblast proliferated, the rate of proliferation of epiblast-derived cells in GFP-negative regions was greater (Figure S4).

Intercalation of cells originating in the visceral endoderm with cells of epiblast origin

The Afp-GFP$^+$ visceral endoderm-derived cells present in the surface layer of embryos could, in principle, reside in one of two alternative conformations: they could either be positioned external to or intercalated among epiblast-derived cells. To determine the relative topology of

these two cell populations, we visualized the basement membrane residing between the outermost cell layer of the embryo and underlying mesoderm by immunohistochemistry (IHC) to fibronectin (Figure 5B–C; E–F). Orthogonal sections and corresponding 3D reconstructions of embryos taken at the ES stage (boxed region, Figure 5A) revealed that the fibronectin network was positioned between the Afp-GFP$^+$ visceral endoderm, and the underlying mesoderm (Figure 5). By the LB stage (boxed region, Figure 5D), when visceral endoderm cells were dispersed, Afp-GFP$^+$ cells (white arrowheads, Figure 5H) were observed adjacent to cells lacking fluorescence (orange arrowheads, Figure 5H). We reasoned that these intercalated GFP-negative cells were of epiblast origin and likely represented cells of the definitive endoderm lineage. We therefore conclude that extensive cell mixing occurs, and that cells of different lineages (visceral endoderm and epiblast) come to occupy a single epithelial layer on the surface layer of the embryo. Our data also revealed that fibronectin occupied ~65% of the total surface area between visceral endoderm and mesoderm at the ES stage, and increased to ~84% by the LB stage (Figure 5B and 5E), suggesting, that there is dynamic remodeling of the basement membrane, which could facilitate cell intercalation.

Remodeling of cell-cell junctions during visceral endoderm cell dispersal

As the visceral endoderm epithelium dispersed, Afp-GFP$^+$ cells transformed from a coherent sheet to isolated single cells. To accomplish this, they must break and reform their nearest-neighbor contacts. We therefore investigated whether remodeling of cell junction proteins in visceral endoderm cells occurred concomitant with their separation. We observed an absence of plasma membrane localized ZO-1, a marker of tight junctions (Hartsock and Nelson, 2007), and a reduction of E-cadherin, a marker of adherens junctions (Hartsock and Nelson, 2007), at the interfaces between neighboring Afp-GFP$^+$ cells undergoing separation (white arrowheads, Figures 5I–5N). We conclude that junctions are being actively remodeled between dispersing visceral endoderm cells.

Visceral endoderm-derived cells are distinct from adjacent epiblast-derived cells

If the outermost layer of the embryo comprised cells of two different origins, we reasoned that molecular differences might exist between these distinct cell populations. Laminin, a basement membrane protein (Tzu and Marinkovich, 2007), coincided with GFP-negative cells, but was absent around Afp-GFP$^+$ cells (white arrowheads, Figure S3). We also observed a differential organization of microtubules, as revealed by the localization of both α- and β-tubulin isoforms (Verhey and Gaertig, 2007), between GFP-negative and Afp-GFP$^+$ cells (white arrowheads, Figure S3), which we interpret as revealing differential cell behaviors in the two populations.

Visceral endoderm-derived cells are incorporated into the gut tube

If the dispersed population of visceral endoderm-derived cells were to persist, it would ultimately contribute to the embryo-proper, specifically to the epithelial lining of the respiratory and digestive tracts and associated organs. Both the *Afp* and *Ttr* cis-regulatory elements are re-activated later in development at around the 20+ somite stage (data not shown and (Kwon et al., 2006)), which precluded analysis of embryos with 20+ somites. However, wholemount imaging of 12–18 somite embryos revealed the presence of Afp-GFP$^+$ cells in the gut tube (Figure 6A). Transverse sections of embryos confirmed the presence of Afp-GFP$^+$ cells with columnar epithelial morphology scattered along the entire length of the gut tube of *Afp::GFP* embryos (Figures 6B–6D). A greater contribution of Afp-GFP$^+$ cells was noted posteriorly, in a region corresponding to the hindgut, which likely represented derivatives of PVE cells overlying the primitive streak (Rivera-Perez and Magnuson, 2005). This was not new expression of the transgene, as *GFP* mRNA could only be detected in the yolk sac at this stage (Figure S5A–S5D).

Cells of similar morphology and distribution were also incorporated along the length of the gut tube in *Ttr::Cre ; R26::lox-neo-lox::LacZ* embryos (Figures 6E–6H) at a time when *Cre* mRNA was mosaic in the yolk sac and absent in the gut (Figure S5E–S5H). Moreover cells in a similar position have been previously reported in 4n <-> 2n chimeras (Hadjantonakis et al., 2002). Quantification of visceral endoderm cell contribution confirmed similar levels along the anterior-posterior length of the gut tube of 12–18 somite stage *Afp::GFP* and *Ttr::Cre ; Z/EG* embryos (Figure 6I–J). Visceral endoderm derived cells comprised less than 10% of the fore- and midgut and approximately 40% of the hindgut at these stages.

Taken together, these data reveal that a population of cells originating in visceral endoderm and positioned distally overlying the epiblast, become intercalated with cells of epiblast origin on the surface layer of the embryo. These visceral endoderm-derived cells continue to divide and are eventually incorporated into the epithelium of the gut tube. If, as we predict, these cells persist within the gut tube, they would represent an extraembryonic lineage contributing to the embryo-proper.

DISCUSSION

We have used genetic labeling and live imaging to visualize the visceral endoderm within the early postimplantation mouse embryo and to document the cell dynamics driving endoderm formation in the mouse gastrula. Our data reveal that the endoderm is formed through a novel morphogenetic mechanism consisting of coordinated visceral endoderm cell dispersal and concomitant epiblast-derived definitive endoderm cell intercalation, and not by mass unidirectional visceral endoderm displacement by emergent definitive endoderm. We demonstrate that the population of visceral endoderm-derived cells overlying the epiblast persist within the endodermal layer of the late gastrula. Visceral endoderm-derived cells are organized around morphologically-distinct midline signaling centers of the embryo including the primitive streak, node and head process. We also note that cells of visceral endoderm origin contribute to the embryonic gut tube, suggesting that the endoderm of the embryo and adult is of dual origin.

Visceral endoderm overlying the epiblast is dispersed but not displaced during gastrulation

Fate mapping and the analysis of molecular markers led to the prevailing model of endoderm formation where the visceral endoderm overlying the epiblast is only transiently associated with the epiblast and is displaced proximally to the visceral yolk sac by the definitive endoderm as it emerges from the anterior primitive streak (Hogan and Zaret, 2002; Lawson et al., 1986; Lawson and Pedersen, 1987; Wells and Melton, 1999). Those earlier studies lacked the spatial and temporal resolution of our analysis, and dynamics were inferred through the analysis of multiple embryos at different time-points.

In contrast to the established model, our data reveal that within a short period of time (<2 hours), cells of the visceral endoderm epithelium overlying the distal two thirds of the epiblast become dispersed (Figure 7). This dispersal is mediated by intercalation of cells originating in the epiblast. The resulting epithelium comprises cells of two distinct origins: the pre-existing visceral endoderm and cells derived from the epiblast. We suggest that this cell behavior is not a simple intercalation between neighboring cells, but a coordinated egression, in which epiblast-derived mesenchymal cells join a pre-existing epithelium, the visceral endoderm (Schock and Perrimon, 2002). Since coordinated widespread egression does not require the unidirectional traction of cells necessary to drive the mass displacement of an epithelial sheet, it represents a novel morphogenetic mechanism for modulating the composition, and rapidly increasing the size of, an epithelium. Such a mechanism would provide the necessary increase in surface area to accomodate the rapid growth of the mouse gastrula.

Conclusions from fate mapping experiments in the chick embryo by Eyal-Giladi and colleagues have many parallels with the current study (Azar and Eyal-Giladi, 1983). During gastrulation, the lower layer of the chick embryo, which is equivalent to the surface layer of the unturned mouse embryo, is mosaic, of cells derived from both the hypoblast and the epiblast (Azar and Eyal-Giladi, 1983). Despite the reduced resolution afforded by their technique, the model they propose for endoderm morphogenesis in the chick is strikingly similar to our model for the mouse.

Previous experiments raised the possibility that epiblast cells might directly populate the visceral endoderm epithelium without first traversing the primitive streak, a possibility which could account for our observations (Tam and Beddington, 1992). However, the absence of epiblast cells or their descendents in the outer layer of most PS-ES stage *Sox2::Cre ; R26::lox-neo-lox::LacZ* embryos suggests that, if epiblast cells do colonize the visceral endoderm directly, this would have to occur after the primitive streak has formed (Figure S6 and data not shown). However, because GFP-negative cells first appear in the surface layer of the embryo after gastrulation is underway (at the LS stage), we favor the possibility that the epiblast-derived cells that incorporate into the visceral endoderm have traversed the primitive streak. If epiblast cells were to egress directly into the visceral endoderm at this stage, they would need to traverse two basement membranes, one between epiblast and mesoderm and another between mesoderm and visceral endoderm, which seems less likely.

Active remodeling of the basement membrane during gastrulation, as indicated by changes in the distribution of fibronectin (Figure 5B and 5E), and the differential localization of laminin (Figure S3A–S3F) could facilitate epiblast cell egression. The analysis of mutants in which gastrulation or endoderm morphogenesis are affected will help elucidate the molecular regulation of this morphogenetic event (Ang and Rossant, 1994; Arnold et al., 2008; Chen et al., 1994; Hart et al., 2002; Kanai-Azuma et al., 2002; Yamaguchi et al., 1994). Future studies will also be needed to address if, as in zebrafish, endodermal progenitors can be retained in the mesoderm layer of the mouse gastrula and incorporated into the endoderm at sites distant from where they traversed the primitive streak (Pezeron et al., 2008).

Since we labelled the entire visceral endoderm with cytoplasmic reporters, we were unable to visualize individual cell behaviors before visceral endoderm cell dispersal. It is therefore possible that rearrangements take place within the visceral endoderm prior to its dispersal. Such movements would include the migration of the anterior visceral endoderm (AVE) which take place at least twenty-four hours before the onset of the visceral endoderm cell dispersal (Figure S7).

Visceral endoderm cells overlying the proximal epiblast contribute to the yolk sac and yolk-sac embryo junction

Egression-mediated cell dispersal occurs in the distal two thirds of the visceral endoderm overlying the epiblast. The proximal third of the visceral endoderm overlying the epiblast is not dispersed nor is it displaced proximally (Movie 8). As egression takes place, the boundary between dispersed and non-dispersed visceral endoderm cells lies distal to the boundary between the embryonic and extraembryonic regions of the conceptus (Figure 1C–1D and Figure S1R), but by the ESom stage these boundaries are coincident (Figure 1G). The initial disparity in the position of the two boundaries and their resolution is in agreement with marker anaylsis and previous studies (Figure S1A, 1D–1E and (Tam et al., 2004)). In this way, the proximal non-dispersed visceral endoderm population overlying the epiblast ends up distal to the embryonic extraembryonic boundary (Movie 9). The resolution of the boundaries consolidates our observations with previous fate-mapping studies, since non-dispersed visceral endoderm-derived cells overlying the proximal epiblast occupy the location of progenitors of the yolk sac endoderm and yolk sac-embryo junction (Lawson et al., 1986;Tam et al., 2004).

Organization of midline visceral endoderm-derived cells around signaling centers

Visceral endoderm-derived cells are organized around midline structures involved in the patterning of embryonic tissues, including the primitive streak, node and head process. Additional experiments will be required to establish if this represents the configuration at the midline coincident with dispersal, or a secondary rearrangement of visceral endoderm cells. Although our observations do not address the dynamic cell behaviors at the midline, it is possible that a specialized population of epiblast-derived cells insert into the visceral endoderm in the vicinity of the node and expands anteriorly along the midline as suggested by previous studies (Lawson et al., 1986; Lawson and Pedersen, 1987; Yamanaka et al., 2007).

The significance of the stereotypical organization of visceral endoderm-derived cells at the midline is not clear, but suggests reciprocal interactions between midline signaling centers and visceral-endoderm derived cells. The maintenance of posterior visceral endoderm (PVE) cells overlying the primitive streak as a coherent sheet that does not disperse is consistent with previous fate mapping data (Lawson and Pedersen, 1987; Tam and Beddington, 1992). The close apposition of the PVE with the primitive streak from the onset of gastrulation through to at least early somite (ESom) stages represents one of the longest tissue associations in the early embryo, the significance of which remains to be determined. Studies in chick also noted the extended association of hypoblast cells with the developing primitive streak and proposed this organization would prolong the mutual inductive influence of the two tissues (Azar and Eyal-Giladi, 1983).

Visceral endoderm-derived cells contribute to the embryo-proper

If a lineage relationship does exist between the visceral endoderm and the endoderm-derived tissues of the fetus, then the segregation of embryonic and extraembryonic lineages, a central feature of early mammalian development, is not as strict as previously believed. The scattered visceral endoderm-derived cells overlying the epiblast divide and do not undergo significant cell death; thus this population appears to be maintained within the embryo-proper.

Our analysis of later 12–18 somite stage embryos revealed the inclusion of visceral endoderm-derived cells within the columnar epithelium of the gut tube. These results are in agreement with our previous observations in 4n <-> 2n chimeras, where the 4n compartment was labeled with a fluorescent reporter under the control of a widespread promoter, which demonstrated the presence of 4n cells within the E9.0 gut tube (Hadjantonakis et al., 2002). Previous fate mapping experiments revealed a small proportion of clones, derived from cells at posterior distal regions on the surface of the embryo, which did contribute to the gut (Lawson and Pedersen, 1987). At the time it was not possible to confirm the origin, nor the final location, of labelled cells using additional molecular markers. It is therefore possible that such clones represent descendents of dispersed visceral endoderm cells. Future studies using genetically induced fate mapping will be needed to follow the descendents of dispersed visceral endoderm cells in later embryos, and to confirm if the gut is of dual origin (Joyner and Zervas, 2006). If, as we suspect, visceral endoderm-derived cells persist within the fetus and adult, it will be important to determine their exact location and whether they are molecularly and functionally distinct from epiblast-derived definitive endoderm cells during homeostasis and disease states.

EXPERIMENTAL PROCEDURES

Transgene construction and strains used

pTtr::RFP and *pTtr::Cre* were generated by inserting either a 1 kb *mRFP1* (Campbell et al., 2002) or 1.1 kb *nlsCre* (Lewandoski et al., 1997) fragments into *pTTR1ExV3* (Costa et al., 1990). Other mouse strains used were: *Afp::GFP* (Kwon et al., 2006), X^{m}/X^{pGFP} (Tg(ACTB-EGFP)D4Nagy/J; JAX #3116) (Hadjantonakis et al., 2001; Hadjantonakis et al., 1998b),

CAG::mRFP1 (B6.Cg-Tg(ACTB-mRFP1)1F1Hadj/J; JAX #5645) (Long et al., 2005); *Sox2::Cre* (Tg(Sox2-cre)1Amc/J; JAX #4783) (Hayashi et al., 2002); *MORE::Cre* (B6.129S4-*Meox2*$^{tm1(cre)Sor}$/J; JAX #3755) (Tallquist and Soriano, 2000); *ROSA26::LNL::LacZ* Cre-reporter (B6;129S4-*Gt(ROSA)*26Sor^{tm1Sor}/J; JAX #3474) (Soriano, 1999), and *Z/EG* Cre reporter (B6.Cg-Tg(ACTB-Bgeo/GFP)21Lbe/J; JAX #3920) (Novak et al., 2000).

Embryo collection for live imaging and processing

Embryos were dissected in PB-1 (Papaioannou and West, 1981; Whittingham and Wales, 1969) containing 10% fetal calf serum and staged according to Downs and Davies (Downs and Davies, 1993). For live imaging, embryos were cultured in 50% rat serum / 50% DMEM-F12 (Jones et al., 2005).

Chimera production

Tetraploid chimeras were generated as described previously (Eakin and Hadjantonakis, 2006; Nagy et al., 2003). Briefly, two tetraploid (4n) *CAG::mRFP1* morula stage embryos were aggregated with R1 or *CAG::GFP* ES cells (Hadjantonakis et al., 1998a; Nagy et al., 1993).

In situ hybridization and immunohistochemistry

Wholemount *in situ* hybridizations were performed according to standard protocols (Nagy et al., 2003). Antisense riboprobes used were for *HNF4α* ((Law and Dugaiczyk, 1981; Vincent and Robertson, 2004), *Afp* (Law and Dugaiczyk, 1981), *Cre*, *GFP* and *RFP*. For sectioning after *in situ* hybridization, embryos were embedded in either 4% low-melt agarose/5% sucrose or 0.4% gelatin/14% BSA/18% sucrose/10% glutaraldehyde, and sectioned at 20–100 μm using a vibrating microtome (Leica VT1000S). For immunohistochemistry (IHC) the following antibodies were used: goat anti-HNF4α (1:300, Santa Cruz), rabbit anti-RFP (1:200, Abcam), mouse anti-ZO-1 (1:300, Zymed), rat anti-E-cadherin (1:300, Sigma), mouse anti-β-catenin (1:300, BD Transduction Laboratories), rabbit anti-laminin (1:300, Rockland Immunochemicals), mouse anti-α-tubulin (1:300, Sigma), mouse anti-β-tubulin (1:300, Sigma), rabbit anti-fibronectin (1:300, Rockland Immunochemicals), or rabbit anti-FoxA2 (1:500, Abcam). Embryos were counterstained with Hoechst for nuclei (Invitrogen) and Phalloidin Alexa546 for F-actin (Invitrogen).

Image acquisition

Widefield images were acquired using a Zeiss Axiocam MRc or MRm camera. Laser scanning confocal data was acquired using a Zeiss LSM510 META. Fluorophores were excited using a 405-nm diode laser (DAPI and Hoechst), 488-nm argon laser (GFP), or 543-nm HeNe laser (Alexa543 and RFP). Objectives used were Plan-Neo 40x/NA1.3, Plan-Apo 20x/NA0.75 and Fluar 5x/NA0.25. Embryos were imaged wholemount in MatTek dishes (Ashland). For live imaging experiments, embryos were maintained in a humidified, temperature-controlled chamber with 5% CO_2 atmosphere. Sections were mounted onto slides and imaged through glass coverslips. Confocal images were acquired as *z*-stacks of *xy* images taken at 0.2-2 μm z-intervals.

Image processing and quantitation

Raw data were processed using AIM software (http://www.zeiss.com/). Digital quantitation of pseudocolored fluorescence was performed using Volocity 4.1 (http://www.improvision.com/). Cell detection and fluorescence intensity measurements were scored by pseudocolor intensity of GFP (green), AlexaFluor546 (red), or Hoechst or DAPI (blue). Thresholds for positive detection were 100±10 for GFP (green), and a total range median for Alexa546 (red) and Hoechst (blue). ROI tool functions were used to calculate areas. Cells were manually counted in Volocity 4.1 software for quantitation of visceral endoderm

contribution to the gut. Time-lapse or image rotation movies were animated in QuickTime Pro (http://www.apple.com/quicktime/).

Supplementary Material

Refer to Web version on PubMed Central for supplementary material.

ACKNOWLEDGEMENTS

We thank the MSKCC Mouse Genetics Core Facility for production of transgenic strains; K. Anderson, M. Baylies, E. Lacy, K. Lawson, J. Rivera-Perez and members of our laboratory for insightful discussions and/or comments on the manuscript. This work was supported by the NIH (RO1-HD052115).

REFERENCES

Andrews GK, Dziadek M, Tamaoki T. Expression and methylation of the mouse alpha-fetoprotein gene in embryonic, adult, and neoplastic tissues. J Biol Chem 1982;257:5148–5153. [PubMed: 6175646]

Ang SL, Rossant J. HNF-3 beta is essential for node and notochord formation in mouse development. Cell 1994;78:561–574. [PubMed: 8069909]

Arnold SJ, Hofmann UK, Bikoff EK, Robertson EJ. Pivotal roles for eomesodermin during axis formation, epithelium-to-mesenchyme transition and endoderm specification in the mouse. Development 2008;135:501–511. [PubMed: 18171685]

Azar Y, Eyal-Giladi H. The retention of primary hypoblastic cells underneath the developing primitive streak allows for their prolonged inductive influence. J Embryol Exp Morphol 1983;77:143–151. [PubMed: 6655430]

Campbell RE, Tour O, Palmer AE, Steinbach PA, Baird GS, Zacharias DA, Tsien RY. A monomeric red fluorescent protein. Proc Natl Acad Sci U S A 2002;99:7877–7882. [PubMed: 12060735]

Chen WS, Manova K, Weinstein DC, Duncan SA, Plump AS, Prezioso VR, Bachvarova RF, Darnell JE Jr. Disruption of the HNF-4 gene, expressed in visceral endoderm, leads to cell death in embryonic ectoderm and impaired gastrulation of mouse embryos. Genes Dev 1994;8:2466–2477. [PubMed: 7958910]

Costa RH, Van Dyke TA, Yan C, Kuo F, Darnell JE Jr. Similarities in transthyretin gene expression and differences in transcription factors: liver and yolk sac compared to choroid plexus. Proc Natl Acad Sci U S A 1990;87:6589–6593. [PubMed: 2395861]

Downs KM, Davies T. Staging of gastrulating mouse embryos by morphological landmarks in the dissecting microscope. Development 1993;118:1255–1266. [PubMed: 8269852]

Dufort D, Schwartz L, Harpal K, Rossant J. The transcription factor HNF3beta is required in visceral endoderm for normal primitive streak morphogenesis. Development 1998;125:3015–3025. [PubMed: 9671576]

Duncan SA, Manova K, Chen WS, Hoodless P, Weinstein DC, Bachvarova RF, Darnell JE Jr. Expression of transcription factor HNF-4 in the extraembryonic endoderm, gut, and nephrogenic tissue of the developing mouse embryo: HNF-4 is a marker for primary endoderm in the implanting blastocyst. Proc Natl Acad Sci U S A 1994;91:7598–7602. [PubMed: 8052626]

Eakin GS, Hadjantonakis AK. Production of chimeras by aggregation of embryonic stem cells with diploid or tetraploid mouse embryos. Nat Protoc 2006;1:1145–1153. [PubMed: 17406396]

Hadjantonakis AK, Cox LL, Tam PP, Nagy A. An X-linked GFP transgene reveals unexpected paternal X-chromosome activity in trophoblastic giant cells of the mouse placenta. Genesis 2001;29:133–140. [PubMed: 11252054]

Hadjantonakis AK, Dickinson ME, Fraser SE, Papaioannou VE. Technicolour transgenics: imaging tools for functional genomics in the mouse. Nat Rev Genet 2003;4:613–625. [PubMed: 12897773]

Hadjantonakis AK, Gertsenstein M, Ikawa M, Okabe M, Nagy A. Generating green fluorescent mice by germline transmission of green fluorescent ES cells. Mech Dev 1998a;76:79–90. [PubMed: 9867352]

Hadjantonakis AK, Gertsenstein M, Ikawa M, Okabe M, Nagy A. Non-invasive sexing of preimplantation stage mammalian embryos. Nat Genet 1998b;19:220–222. [PubMed: 9662390]

Hadjantonakis AK, Macmaster S, Nagy A. Embryonic stem cells and mice expressing different GFP variants for multiple non-invasive reporter usage within a single animal. BMC Biotechnol 2002;2:11. [PubMed: 12079497]

Hart AH, Hartley L, Sourris K, Stadler ES, Li R, Stanley EG, Tam PP, Elefanty AG, Robb L. Mixl1 is required for axial mesendoderm morphogenesis and patterning in the murine embryo. Development 2002;129:3597–3608. [PubMed: 12117810]

Hartsock A, Nelson WJ. Adherens and tight junctions: Structure, function and connections to the actin cytoskeleton. Biochim Biophys Acta. 2007

Hayashi S, Lewis P, Pevny L, McMahon AP. Efficient gene modulation in mouse epiblast using a Sox2Cre transgenic mouse strain. Mech Dev 2002;119:S97–S101. [PubMed: 14516668]

Hogan, BLM.; Zaret, KS. Development of the Endoderm and Its Tissue Derivatives. In: Rossant, J.; Tam, PL., editors. Mouse Development. New York: Academic Press; 2002.

Jones, EAV.; Hadjantonakis, AK.; Dickinson, ME. Imaging Mouse Embryonic Development. In: Yuste, R.; Konnerth, A., editors. Imaging in Neuroscience and Development. Cold Spring Harbor, NY: Cold Spring Harbor Laboratory Press; 2005.

Joyner AL, Zervas M. Genetic inducible fate mapping in mouse: establishing genetic lineages and defining genetic neuroanatomy in the nervous system. Dev Dyn 2006;235:2376–2385. [PubMed: 16871622]

Kanai-Azuma M, Kanai Y, Gad JM, Tajima Y, Taya C, Kurohmaru M, Sanai Y, Yonekawa H, Yazaki K, Tam PP, Hayashi Y. Depletion of definitive gut endoderm in Sox17-null mutant mice. Development 2002;129:2367–2379. [PubMed: 11973269]

Kinder SJ, Tsang TE, Quinlan GA, Hadjantonakis AK, Nagy A, Tam PP. The orderly allocation of mesodermal cells to the extraembryonic structures and the anteroposterior axis during gastrulation of the mouse embryo. Development 1999;126:4691–4701. [PubMed: 10518487]

Krumlauf R, Hammer RE, Tilghman SM, Brinster RL. Developmental regulation of alpha-fetoprotein genes in transgenic mice. Mol Cell Biol 1985;5:1639–1648. [PubMed: 2410773]

Kwon GS, Fraser ST, Eakin GS, Mangano M, Isern J, Sahr KE, Hadjantonakis AK, Baron MH. Tg(Afp-GFP) expression marks primitive and definitive endoderm lineages during mouse development. Dev Dyn 2006;235:2549–2558. [PubMed: 16708394]

Law SW, Dugaiczyk A. Homology between the primary structure of alpha-fetoprotein, deduced from a complete cDNA sequence, and serum albumin. Nature 1981;291:201–205. [PubMed: 6164927]

Lawson KA, Meneses JJ, Pedersen RA. Cell fate and cell lineage in the endoderm of the presomite mouse embryo, studied with an intracellular tracer. Dev Biol 1986;115:325–339. [PubMed: 3709966]

Lawson KA, Meneses JJ, Pedersen RA. Clonal analysis of epiblast fate during germ layer formation in the mouse embryo. Development 1991;113:891–911. [PubMed: 1821858]

Lawson KA, Pedersen RA. Cell fate, morphogenetic movement and population kinetics of embryonic endoderm at the time of germ layer formation in the mouse. Development 1987;101:627–652. [PubMed: 3502998]

Lewandoski M. Conditional control of gene expression in the mouse. Nat Rev Genet 2001;2:743–755. [PubMed: 11584291]

Lewandoski M, Wassarman KM, Martin GR. Zp3-cre, a transgenic mouse line for the activation or inactivation of loxP-flanked target genes specifically in the female germ line. Curr Biol 1997;7:148–151. [PubMed: 9016703]

Lewis SL, Tam PP. Definitive endoderm of the mouse embryo: formation, cell fates, and morphogenetic function. Dev Dyn 2006;235:2315–2329. [PubMed: 16752393]

Lin TP, Labosky PA, Grabel LB, Kozak CA, Pitman JL, Kleeman J, MacLeod CL. The Pem homeobox gene is X-linked and exclusively expressed in extraembryonic tissues during early murine development. Dev Biol 1994;166:170–179. [PubMed: 7958444]

Long JZ, Lackan CS, Hadjantonakis AK. Genetic and spectrally distinct in vivo imaging: embryonic stem cells and mice with widespread expression of a monomeric red fluorescent protein. BMC Biotechnol 2005;5:20. [PubMed: 15996270]

Mesnard D, Guzman-Ayala M, Constam DB. Nodal specifies embryonic visceral endoderm and sustains pluripotent cells in the epiblast before overt axial patterning. Development 2006;133:2497–2505. [PubMed: 16728477]

Nagy, A.; Gertsenstein, M.; Vintersten, K.; Behringer, R. Manipulating the Mouse Embryo. Vol. Third edn. Cold Spring Harbor: Cold Spring Harbor Laboratory Press; 2003.

Nagy A, Rossant J, Nagy R, Abramow-Newerly W, Roder JC. Derivation of completely cell culture-derived mice from early-passage embryonic stem cells. Proc Natl Acad Sci U S A 1993;90:8424–8428. [PubMed: 8378314]

Novak A, Guo C, Yang W, Nagy A, Lobe CG. Z/EG, a double reporter mouse line that expresses enhanced green fluorescent protein upon Cre-mediated excision. Genesis 2000;28:147–155. [PubMed: 11105057]

Papaioannou VE, West JD. Relationship between the parental origin of the X chromosomes, embryonic cell lineage and X chromosome expression in mice. Genet Res 1981;37:183–197. [PubMed: 7262553]

Parameswaran M, Tam PP. Regionalisation of cell fate and morphogenetic movement of the mesoderm during mouse gastrulation. Dev Genet 1995;17:16–28. [PubMed: 7554492]

Pezeron G, Mourrain P, Courty S, Ghislain J, Becker TS, Rosa FM, David NB. Live analysis of endodermal layer formation identifies random walk as a novel gastrulation movement. Curr Biol 2008;18:276–281. [PubMed: 18291651]

Rivera-Perez JA, Mager J, Magnuson T. Dynamic morphogenetic events characterize the mouse visceral endoderm. Dev Biol 2003;261:470–487. [PubMed: 14499654]

Rivera-Perez JA, Magnuson T. Primitive streak formation in mice is preceded by localized activation of Brachyury and Wnt3. Dev Biol 2005;288:363–371. [PubMed: 16289026]

Rodriguez TA, Srinivas S, Clements MP, Smith JC, Beddington RS. Induction and migration of the anterior visceral endoderm is regulated by the extra-embryonic ectoderm. Development 2005;132:2513–2520. [PubMed: 15857911]

Schock F, Perrimon N. Molecular mechanisms of epithelial morphogenesis. Annu Rev Cell Dev Biol 2002;18:463–493. [PubMed: 12142280]

Soriano P. Generalized lacZ expression with the ROSA26 Cre reporter strain. Nat Genet 1999;21:70–71. [PubMed: 9916792]

Srinivas S. The anterior visceral endoderm-turning heads. Genesis 2006;44:565–572. [PubMed: 17078044]

Tallquist MD, Soriano P. Epiblast-restricted Cre expression in MORE mice: a tool to distinguish embryonic vs. extra-embryonic gene function. Genesis 2000;26:113–115. [PubMed: 10686601]

Tam PP, Beddington RS. The formation of mesodermal tissues in the mouse embryo during gastrulation and early organogenesis. Development 1987;99:109–126. [PubMed: 3652985]

Tam PP, Beddington RS. Establishment and organization of germ layers in the gastrulating mouse embryo. Ciba Found Symp 1992;165:27–41. [PubMed: 1516473]discussion 42-29

Tam PP, Khoo PL, Wong N, Tsang TE, Behringer RR. Regionalization of cell fates and cell movement in the endoderm of the mouse gastrula and the impact of loss of Lhx1(Lim1) function. Dev Biol 2004;274:171–187. [PubMed: 15355796]

Tam PP, Rossant J. Mouse embryonic chimeras: tools for studying mammalian development. Development 2003;130:6155–6163. [PubMed: 14623817]

Taraviras S, Monaghan AP, Schutz G, Kelsey G. Characterization of the mouse HNF-4 gene and its expression during mouse embryogenesis. Mech Dev 1994;48:67–79. [PubMed: 7873404]

Thomas P, Beddington R. Anterior primitive endoderm may be responsible for patterning the anterior neural plate in the mouse embryo. Curr Biol 1996;6:1487–1496. [PubMed: 8939602]

Tilghman SM, Belayew A. Transcriptional control of the murine albumin/alpha-fetoprotein locus during development. Proc Natl Acad Sci U S A 1982;79:5254–5257. [PubMed: 6182563]

Tremblay KD, Zaret KS. Distinct populations of endoderm cells converge to generate the embryonic liver bud and ventral foregut tissues. Dev Biol 2005;280:87–99. [PubMed: 15766750]

Tzu J, Marinkovich MP. Bridging structure with function: Structural, regulatory, and developmental role of laminins. Int J Biochem Cell Biol. 2007

Verhey KJ, Gaertig J. The tubulin code. Cell Cycle 2007;6:2152–2160. [PubMed: 17786050]

Wells JM, Melton DA. Vertebrate endoderm development. Annu Rev Cell Dev Biol 1999;15:393–410. [PubMed: 10611967]

Whittingham DG, Wales RG. Storage of two-cell mouse embryos in vitro. Australian Journal of Biological Sciences 1969;22:1065–1068. [PubMed: 5374532]

Yamaguchi TP, Harpal K, Henkemeyer M, Rossant J. fgfr-1 is required for embryonic growth and mesodermal patterning during mouse gastrulation. Genes Dev 1994;8:3032–3044. [PubMed: 8001822]

Yamamura K, Miki T, Suzuki N, Ebihara T, Kawai K, Kumahara Y, Honjo T. Introduction of mouse C epsilon genes into Cos-7 cells and fertilized mouse eggs. J Biochem (Tokyo) 1985;97:333–339. [PubMed: 2987199]

Yamanaka Y, Tamplin OJ, Beckers A, Gossler A, Rossant J. Live imaging and genetic analysis of mouse notochord formation reveals regional morphogenetic mechanisms. Dev Cell 2007;13:884–896. [PubMed: 18061569]

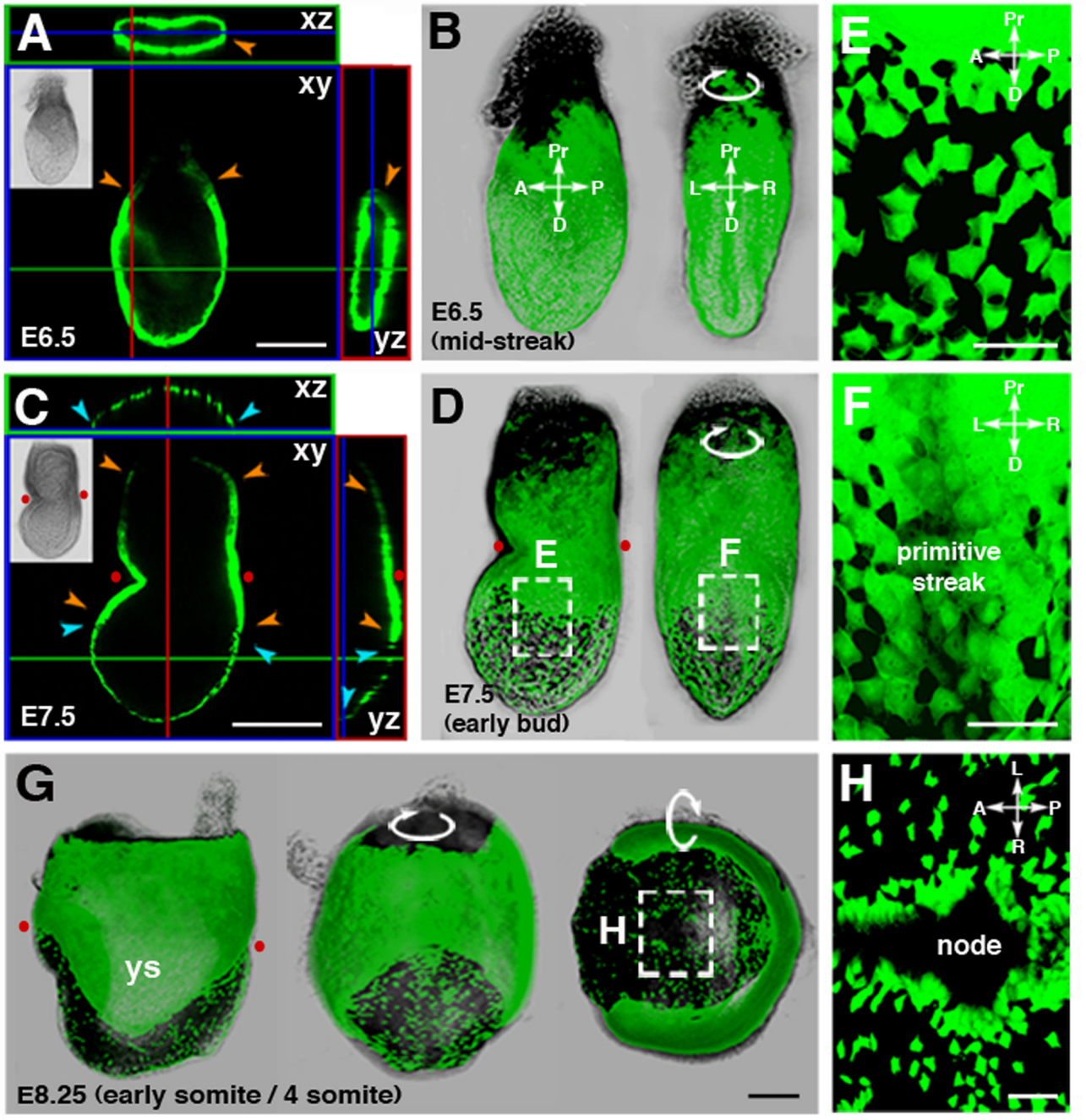

Figure 1. Genetic-labeling and live imaging endoderm morphogenesis

(A and B) At the onset of gastrulation, the visceral endoderm encapsulates the epiblast and extraembryonic ectoderm. (A) Orthogonal sections through an E6.5 (MS stage) embryo. (B) 3D reconstruction of *z*-stack shown in A projected as a lateral (left) and posterior (right) view. (C and D) By E7.5 (EB stage) visceral endoderm cells overlying the extraembryonic ectoderm form a contiguous sheet of cells and are sparsely distributed overlying the epiblast. (C) Orthogonal sections reveal contiguous GFP fluorescence overlying the extraembryonic ectoderm (outlined by orange arrowheads) and interrupted GFP fluorescence overlying the distally positioned epiblast and its derivatives (outlined by blue arrowheads). (D) 3D reconstruction of *z*-stack shown in C projected as a lateral (left) and a posterior (right) view.

(E) High magnification view of a region on the left lateral side of the embryo and (F) overlying the primitive streak.
(G) 3D reconstruction of a *z*-stack taken though an E8.25 (ESom stage) embryo, projected as lateral (left), and posterior (center), and ventral views (right
(H) High magnification views of the region around node.
Red dots correspond to the position of the amnion, the morphological landmark of the boundary between the extraembryonic and embryonic part of the conceptus. ys, yolk sac; Pr, proximal; D, distal; A, anterior; P, posterior; L, left; R, right. Scale bars = 100 μm in A; 200 μm in C and G; 50 μm in E, F, and H.

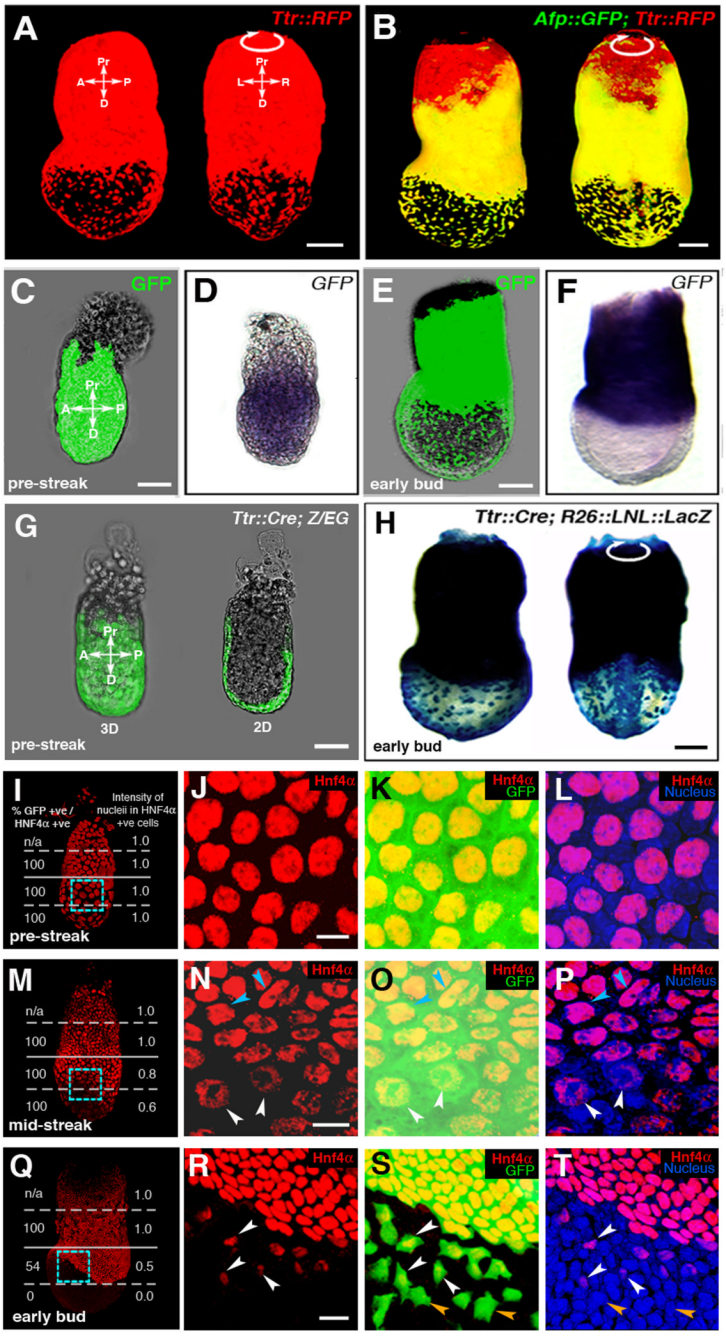

Figure 2. Fluorescent proteins as cell tracers in visceral endoderm derived cells that are downregulating marker genes

(A and B) Two distinct visceral endoderm-specific *cis*-regulatory elements identify the same population of cells. (A) 3D reconstruction of *z*-stack acquired from an EB stage (E7.5) *Ttr::RFP*$^{Tg/+}$ transgenic projected laterally (left) and posteriorly (right). (B) 3D reconstruction of *z*-stack from an *Afp::GFP*$^{Tg/+}$; *Ttr::RFP*$^{Tg/+}$ transgenic projected laterally (left) and posteriorly (right). Co-expressing cells are yellow.

(C–F) Localization of GFP protein (green fluorescence, C and E) and mRNA (blue staining, D and F) in PS and EB stage *Afp::GFP*$^{Tg/+}$ embryos. (C and D) PS stage embryo imaged live

for GFP protein (C), then processed for *GFP* mRNA *in situ* hybridization (D). (E and F) EB stage embryo imaged live (E), then processed for mRNA *in situ* hybridization (F).
(G and H) *Cre* recombinase-mediated excision labels the entire visceral endoderm at PS stages in *Ttr::Cre*$^{Tg/+}$ *; Z/EG* embryos (green fluorescence, G), while visceral endoderm-derived cells overlying the epiblast is labeled in *Ttr::Cre*$^{Tg/+}$; *R26::LNL::LacZ*$^{+/-}$ embryos at the EB stage (blue staining, H).
IHC of PS stage (I–L), MS stage (M–P) and EB stage (Q–T) *Afp::GFP*$^{Tg/+}$ embryos. GFP (green), Hnf4α (red) and Hoechst (labeling nuclei - blue). (I, M and Q) 3D reconstructions of *z*-stacks quantifying Hnf4a expression in distinct regions of each embryo. Percentage of GFP^{+} cells that are also Hnf4a+ (left column); average fluorescence intensity of Hnf4a^{+} nuclei (right column). High-magnification 3D single and merged channel views of boxed regions (J–L, N–P and R–T). GFP^{+} cells with high levels of Hnf4α (blue arrowheads), GFP^{+} cells expressing reduced levels of Hnf4α (white arrowheads), GFP^{+} cells with no detectable Hnf4α (orange arrowheads). Pr, proximal; D, distal; A, anterior; P, posterior; L, left; R, right; 3D, 3-dimensions; 2D, 2-dimensions. Scale bars = 20 μm in J,N and R; 50 μm in C and G; 100 μm in A,B,E and H.

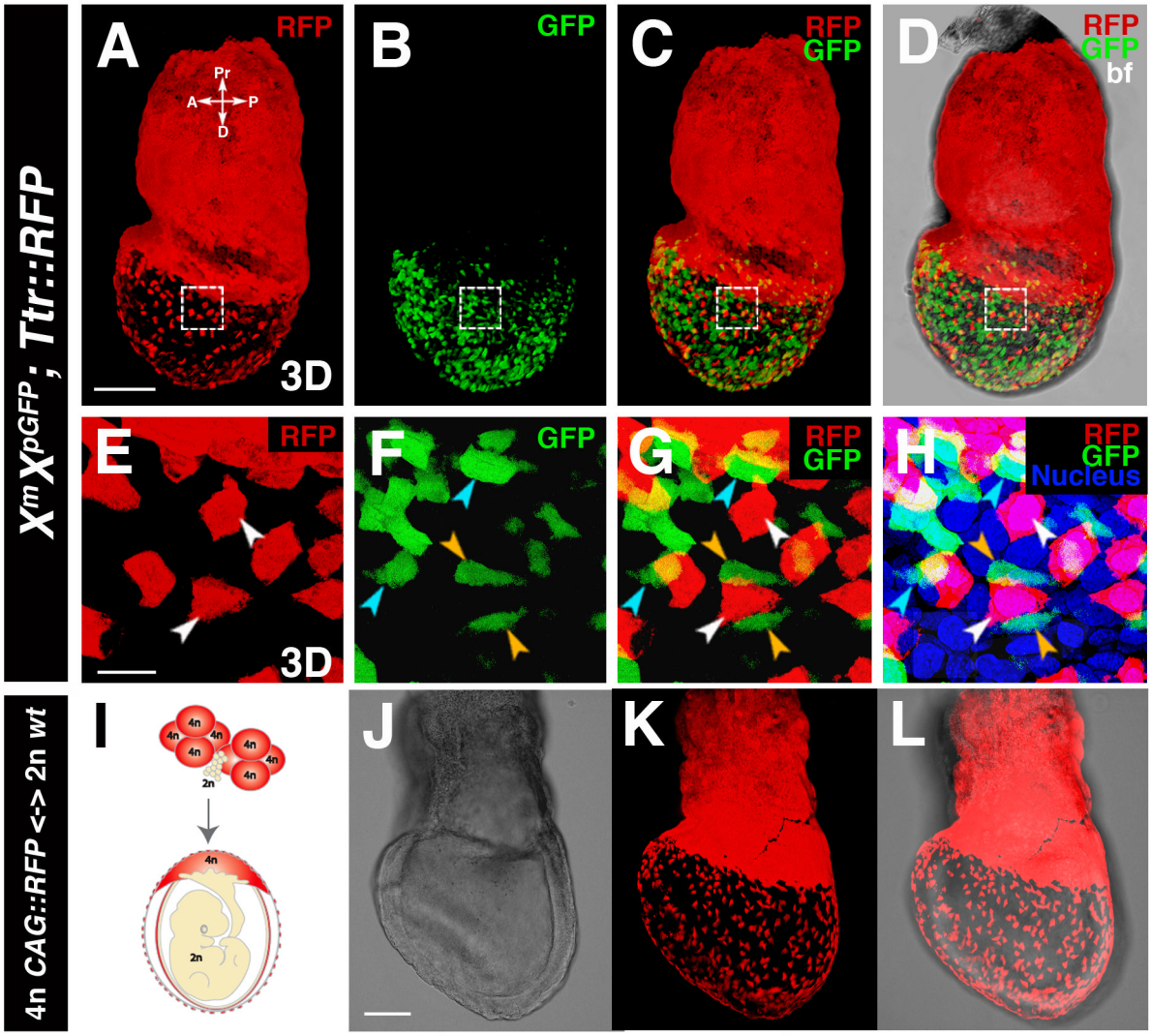

Figure 3. A scattered population of cells located in the surface layer of the embryo overlying the epiblast is not of epiblast origin

(A–H) 3D reconstructions of laser scanning confocal *z*-stacks taken through an LB stage X^mX^{pGFP}; $Ttr::RFP^{Tg/+}$ embryo. (E–H) High magnification views of boxed region. RFP^+ cells all of which are located on the surface of the embryo (white arrowheads); GFP^+ cells located on the surface of the embryo (orange arrowheads); GFP^+ cells that are not superficially located (blue arrowheads).

(I–L) EHF stage 4n $CAG::RFP^{Tg/+}$ <-> 2n R1 ES cell chimera. Schematic depicting the contribution of tetraploid and diploid compartments (I). Brightfield image (J), 3D reconstruction of *z*-stack of mages acquired in red fluorescent channel (K), and overlay (L). Dispersed population of 4n RFP^+ cells overlying the epiblast (white arrowheads). Scale bars = 200 μm in A; 20 μm in E; 100 μm in J.

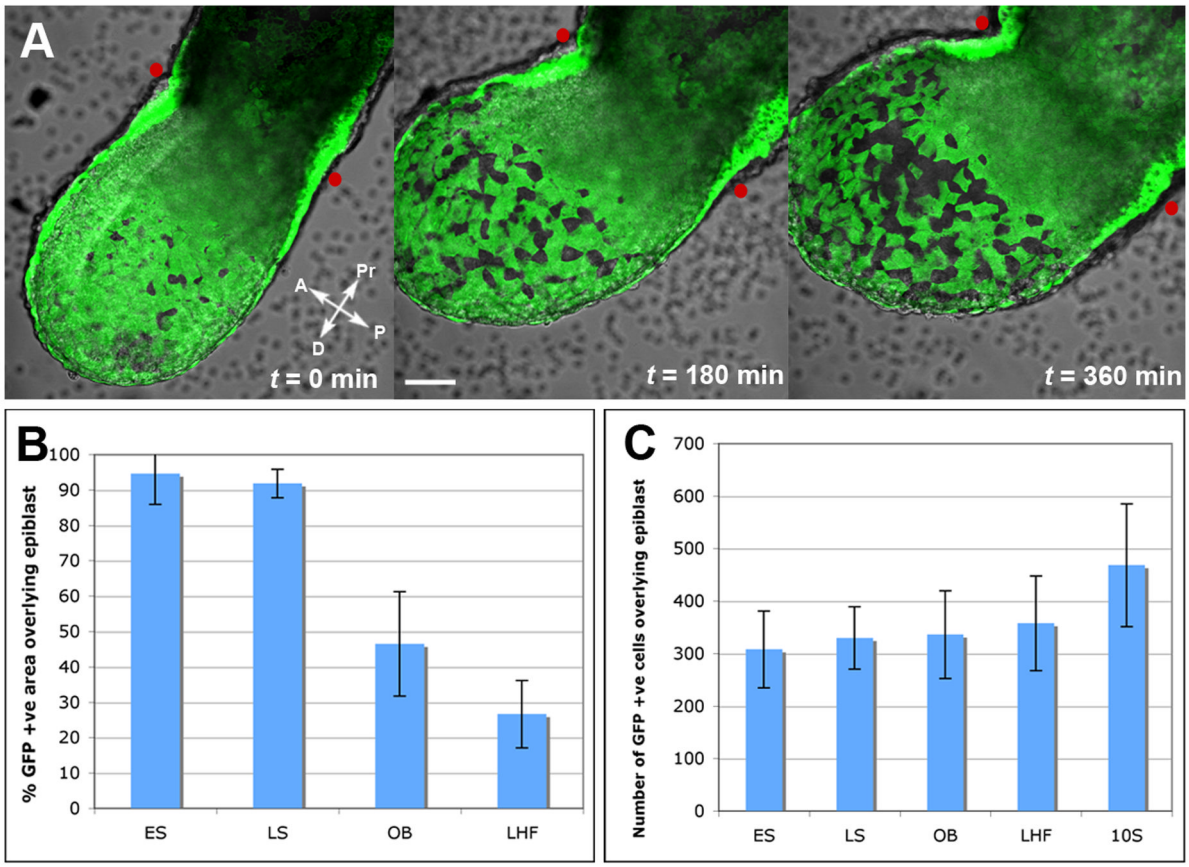

Figure 4. Dynamics of visceral endoderm cell dispersal

(A) Still images from 3D time-lapse movie (Supplementary movie 8) of an *Afp::GFP*$^{Tg/+}$ embryo from LS to EB stage. Red dots correspond to the position of the amnion, the morphological landmark of the boundary between the extraembryonic and embryonic part of the conceptus. Scale bar = 50μm.

(B) Histograms depicting fluorescence area overlying the epiblast in ES (N=7), LS (N=6), OB (N=20), to LHF (N=5) stages.

(C) Histograms depicting GFP^{+} cells overlying the epiblast at 10 somite (10S, N=9) stage.

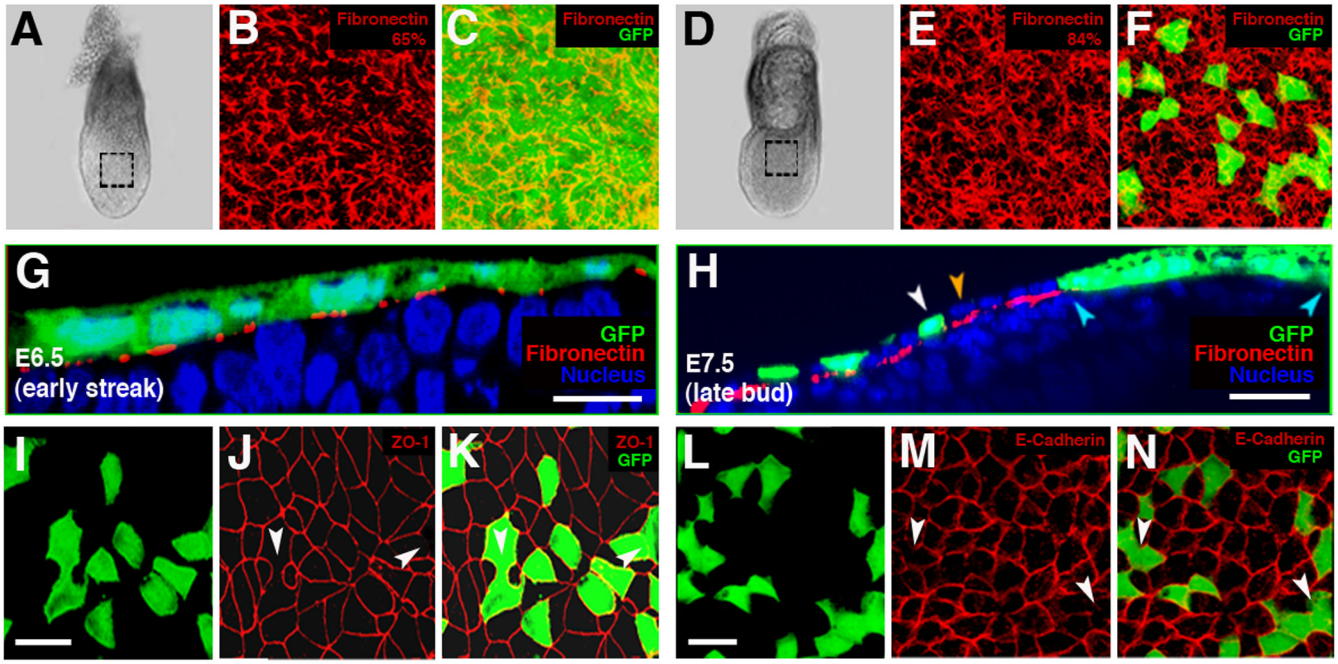

Figure 5. Intercalation of epiblast-derived and visceral endoderm cells on the surface of the embryo

(A, D) Wholemount view of ES (A) and EB (D) stage embryos used for IHC to fibronectin.

(B–C and E–F) 3D reconstruction of *z*-stacks in boxed region of A (B–C) or D (E–F), depicting a filamentous fibronectin network. Percentages in (B) and (E) depict density of fibronectin as quantified by positive area of red channel under equal threshold and magnification in the two embryonic stages.

(G) *yz* view of EB stage *Afp::GFP*$^{Tg/+}$ embryo reveals a contiguous sheet of GFP^{+} cells covering the fibronectin matrix (red) on the surface.

(H) *yz* view of LB stage *Afp::GFP*$^{Tg/+}$ embryo reveals intercalation of GFP^{+} and GFP^{-} cells at the LB stage. Isolated GFP^{+} cells (white arrowheads); GFP^{-} cells neighboring isolated GFP^{+} cells positioned on the same side of the fibronectin matrix (orange arrowheads).

(I–K) 3D reconstructed *z*-stacks taken through the region overlying the epiblast of LB (E7.5) stage *Afp::GFP*$^{Tg/+}$ embryo visualized for ZO-1. Interfaces lacking ZO-1 (white arrowheads).

(L–N) 3D reconstructed *z*-stacks through the region overlying the epiblast of LB (E7.5) stage *Afp::GFP*$^{Tg/+}$ embryo visualized for E-cadherin. Junctions exhibiting reduced E-cadherin (white arrowheads). Scale bars = 50 μm.

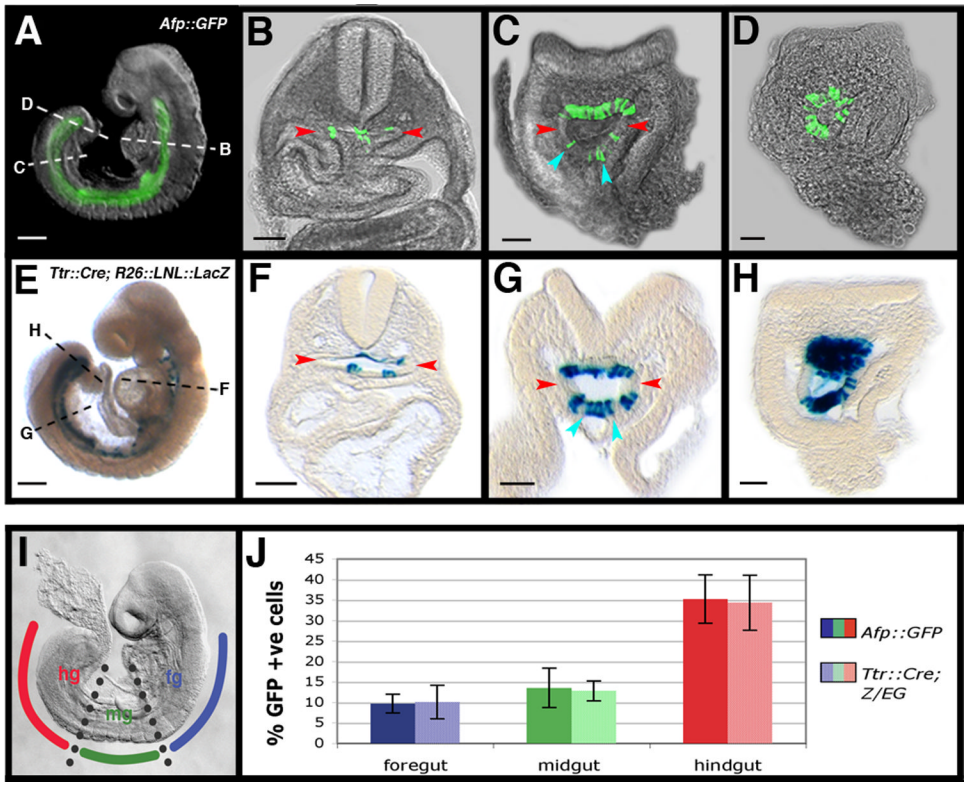

Figure 6. Cells originating in the visceral endoderm contribute to the embryonic gut

(A) Wholemount view of a 14 somite stage (E8.75) *Afp::GFP*$^{Tg/+}$ embryo.

(B–D) Transverse sections at different rostrocaudal levels (dashed lines) though the embryo in A.

(E) Wholemount view of a 15 somite stage (E8.75) *Ttr::Cre*$^{Tg/+}$ *; R26::LNL::LacZ*$^{+/-}$ embryo.

(F–H) Transverse sections at different rostrocaudal levels (indicated by dashed lines) though the embryo in E. Individual visceral endoderm-derived cells with columnar epithelial morphology constitute part of the hindgut (blue arrowheads); lateral extremities of the gut tube devoid of visceral endoderm-derived cells (red arrowheads). Scale bars = 200 μm in A and E; 100 μm in B–D and F–H.

(I) Diagram illustrating the subdivision of gut tube into foregut (fg), midgut (mg), and hindgut (hg) in a 15 somite stage (E8.75) embryo.

(J) Histograms of visceral endoderm cell contribution to the gut in 14–18 somite stage (E8.75) *Afp::GFP*$^{Tg/+}$ and *Ttr::Cre*$^{Tg/+}$ *; Z/EG*$^{Tg/+}$ embryos. N = 8, 7, 7, 9, 11, and 7 in sequential left-to-right order of bars.

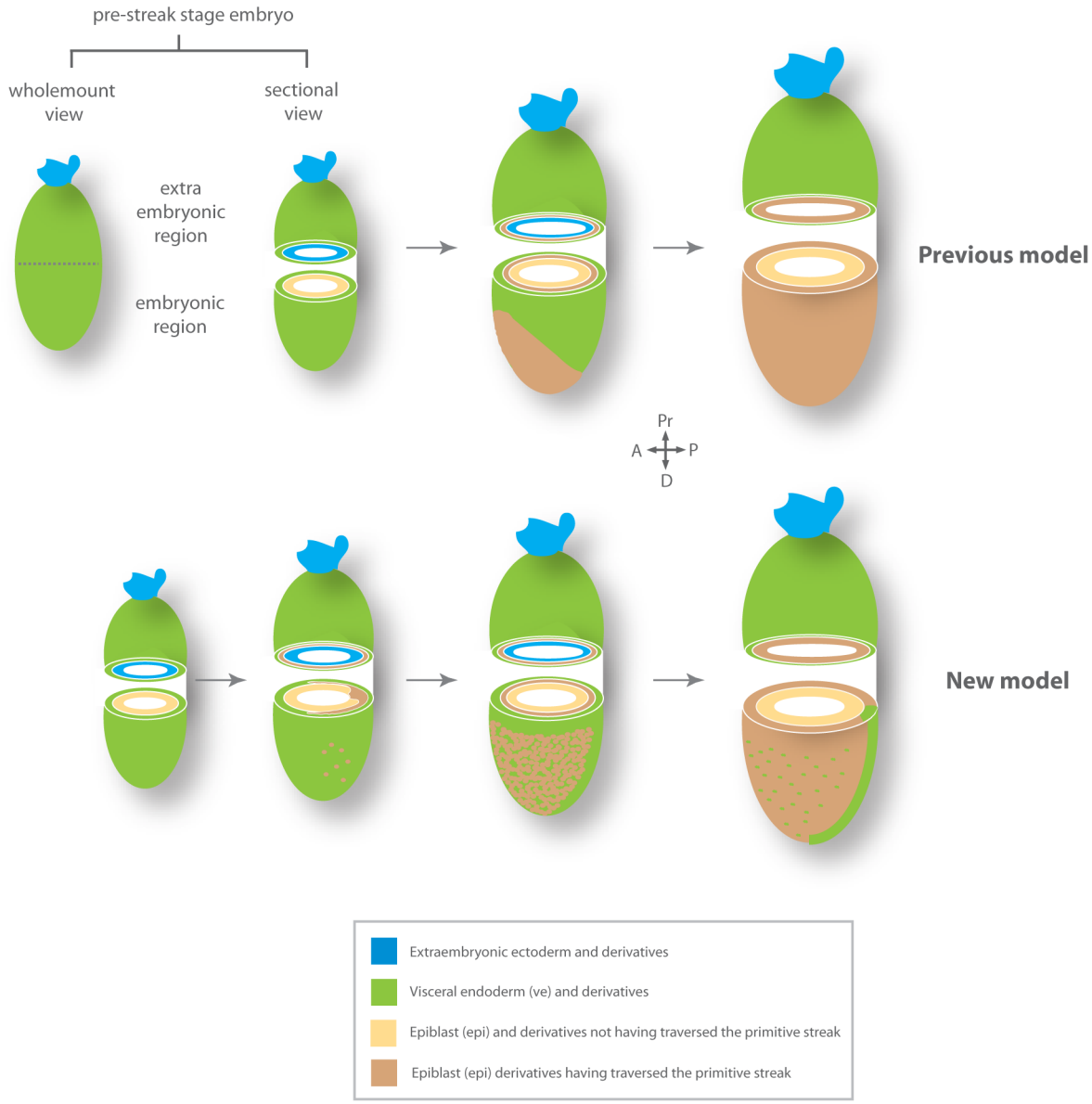

Figure 7. Models for endoderm morphogenesis in the mouse gastrula

Definitive endoderm arising at the anterior primitive streak located at the distal tip of the embryo in the vicinity of the node (previous model). As the definitive endoderm emerges, the visceral endoderm is displaced proximally towards the extraembryonic region.
Visceral endoderm overlying the epiblast becomes dispersed by widespread intercalation of epiblast-derived cells (new model).